



Magnetotelluric (MT) Data – 3D Inversion Modeling Eastern Tasmania, Australia

**3D Modeling Report 2010
*Volume 1 of 1***

**Prepared for
KUTh Energy Ltd.**

**By
Geosystem Srl
WesternGeco EM
Milan, Italy**



Effective date: May 2010

Revision History:

Rev. No.	Effective Date	Description	Prepared by	Reviewed by	Approved by
01	20 April 2010	Draft	Wolfgang Soyer		
02	05 May 2010		Alessandra Battaglini		
03	21 May 2010	Final Version		Wolfgang Soyer	Stephen Hallinan

CONTENTS

SUMMARY	1
1 SURVEY LOCATION	2
2 DATA CHARACTERISTICS.....	4
2.1 Sounding Curves	4
2.2 Parameter Maps.....	6
2.3 Induction Vectors.....	7
3 MT MODELING – 3D INVERSION.....	9
3.1 Mesh Dimensions.....	9
3.2 Data Input	10
3.3 Inversion Parameters	11
3.4 Data Fit	11
3.5 Modeling Results.....	13
4 BIBLIOGRAPHY	23
Appendix A GLOSSARY.....	A-1
Appendix B 3D MT INVERSION MODELING	B-1
B.1 3D Forward Modeling	B-1
B.2 3D Inversion.....	B-1
Appendix C INVERSION HISTORY	C-1
Appendix D DIGITAL DATA.....	D-1
D.1 Content	D-1
D.2 Output Data Formats	D-1
D.2.1 Model File	D-1
D.2.2 Predicted Data.....	D-3
D.2.3 Inversion Log and Data Misfit.....	D-3
Appendix E RESISTIVITY PLATES AND CROSS SECTIONS	E-1
E.1 Maps.....	E-1
E.2 Cross Sections.....	E-1

FIGURES

Figure 1. Resistivity depth map at -2000m msl from the 2010 3D MT inversion result.....	1
Figure 2. MT station and profile locations on topographic base map. Sites included in the 2010 3D MT inversion are marked in color.	2
Figure 3. Example soundings STL022A and NSB034A from the 2008-2009 data set (upper panel) and Site20A and Site36A from the 2010 data set (lower panel). Data are rotated to N106°E, the rotation angle for the 3D modelling. Off-diagonal components xy (red) and yx (blue) are displayed in bold colors, on-diagonal tensor elements are in faint colours (xx and yy), and masked data in gray.	5
Figure 4. Example tipper curves of the 2010 data set: Site28A, Site32A (top), and Site20A, Site30A (bottom), after initial data masking (Geosystem). Real parts are shown in red, imaginary in blue.	6
Figure 5. Impedance phase Invariant for the combined 2008-9 and 2010 MT data set at frequencies 100Hz, 10Hz, 1Hz, and 0.1Hz.	7
Figure 6. Real induction vectors for 10Hz, 1Hz, 0.1Hz and 0.01Hz (top left to right bottom). Arrows are plotted in the convention pointing towards conductors. Black dashed lines show how high conductivity is indicated at major fault locations.	8
Figure 7. Plan views of full 3D model meshes (LHS) and fine mesh centred on MT station locations (RHS). Background grid is topography (SRTM DEM).	10
Figure 8. Section views of full and core 3D model mesh (LHS, RHS), showing also the intersection with the elevation grid (RHS).	10
Figure 9. Example MT soundings NSA014A, SITE20A and NSB044A show fit between observed (LHS) and calculated 3D model response (RHS). Data are rotated in 3D mesh direction. Note the final resistivity model reproduces the static shifts inherent in the MT data at NSA014A, both through inclusion of near-surface structure and direct static shift factors.	12
Figure 10. Resistivity depth maps from -500 to -3000m msl from the 2010 3D MT inversion (from top left to bottom right). Blue sites are from the new 2010 data set. The dashed black lines at elevations -1500m and -2500m msl mark the high conductivity trends inferred from induction vector maps at 0.1Hz dan 0.01Hz, respectively (, Figure 5.	14
Figure 11. Resistivity depth maps at -1500 and -3000m msl from 3D MT inversion compared to the 2009 results (bottom). Blue sites are from the new 2010 data set.	15
Figure 12. Cross section along profile “A” through the 3D resistivity model (NW to SE, top), compared to the 2009 inversion result (bottom).	16
Figure 13. Cross section along profile “B” through the 3D resistivity model (NE to SW, top), compared to the 2009 inversion result (bottom).	17

Figure 14. Cross section along profile “C” through the 3D resistivity model (NE to SW, top), compared to the 2009 inversion result (bottom).....	18
Figure 15. Cross section along profiles “B1”, “D” and “D1” through the 3D resistivity model (N is to the left). Blue sites are from the new 2010 data set.	19
Figure 16. Cross section along profile “D” through the 3D resistivity model (NE to SW, top), compared to the 2009 inversion result (bottom). Blue sites are from the new 2010 data set.	20
Figure 17. Cross-sections along profiles “EW-2”, “EW-11”, and “EW-1” (top to bottom) through the 3D resistivity model (W is to the left). Blue sites are from the new 2010 data set.	21
Figure 18. Cross section along profile “EW-1” through the 3D resistivity model (top), compared to the 2009 inversion result (bottom). Blue sites are from the new 2010 data set.....	22

SUMMARY

Under agreement from 24 Feb, 2010 with KUTh Energy Ltd., WesternGeco's Land EM group Geosystem carried out full tensor 3D inversion modelling of a passive magnetotelluric (MT) data set from 2008, 2009 and 2010, comprising 244 soundings in eastern Tasmania.

The 2008-2009 data sets were 3D modelled in 2009 by Geosystem. Most of these data are located along three profiles at nominally 1km spacing inline, with about 30 stations off the lines at 5-10km spacing. The new 2010 data set of 43 sites integrated in this study provides better 3D coverage around the two SSW-NNE lines.

The data were inverted for resistivity structure by 3D MT inversion modeling, using the same area of the 2009 inversion model, with in total $121 \times 99 \times 112 \approx 1.3\text{M}$ cells and an 800m lateral vs. 100m vertical (at depth) cell size. 238 MT sites were judged to be of sufficient quality for inclusion in the 3D inversion procedure.

3D inversion results, largely agree with the 2009 inversion results along the 3 main lines, where they are also most reliable. Due to the newly integrated 2010 data set, structure between the lines is now better resolved. In particular, a strong E-W aligned conductivity contrast is modelled in the southern area, similarly seen in induction vectors and roughly coincident with fault locations.

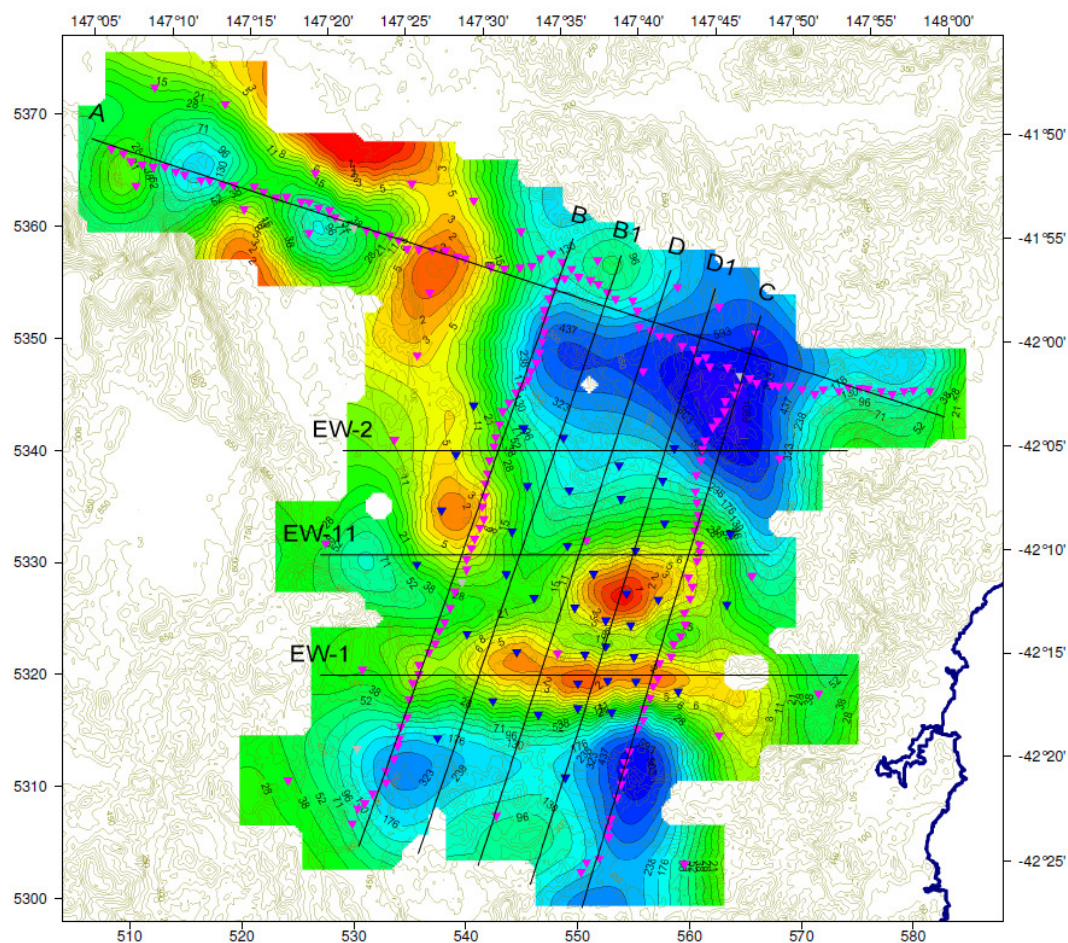


Figure 1. Resistivity depth map at -2000m msl from the 2010 3D MT inversion result.

1 SURVEY LOCATION

An MT survey of in total 244 stations was carried out in eastern Tasmania in 2008, 2009, and 2010. A subset of 238 sites was included in the 2010 3D MT inversion.

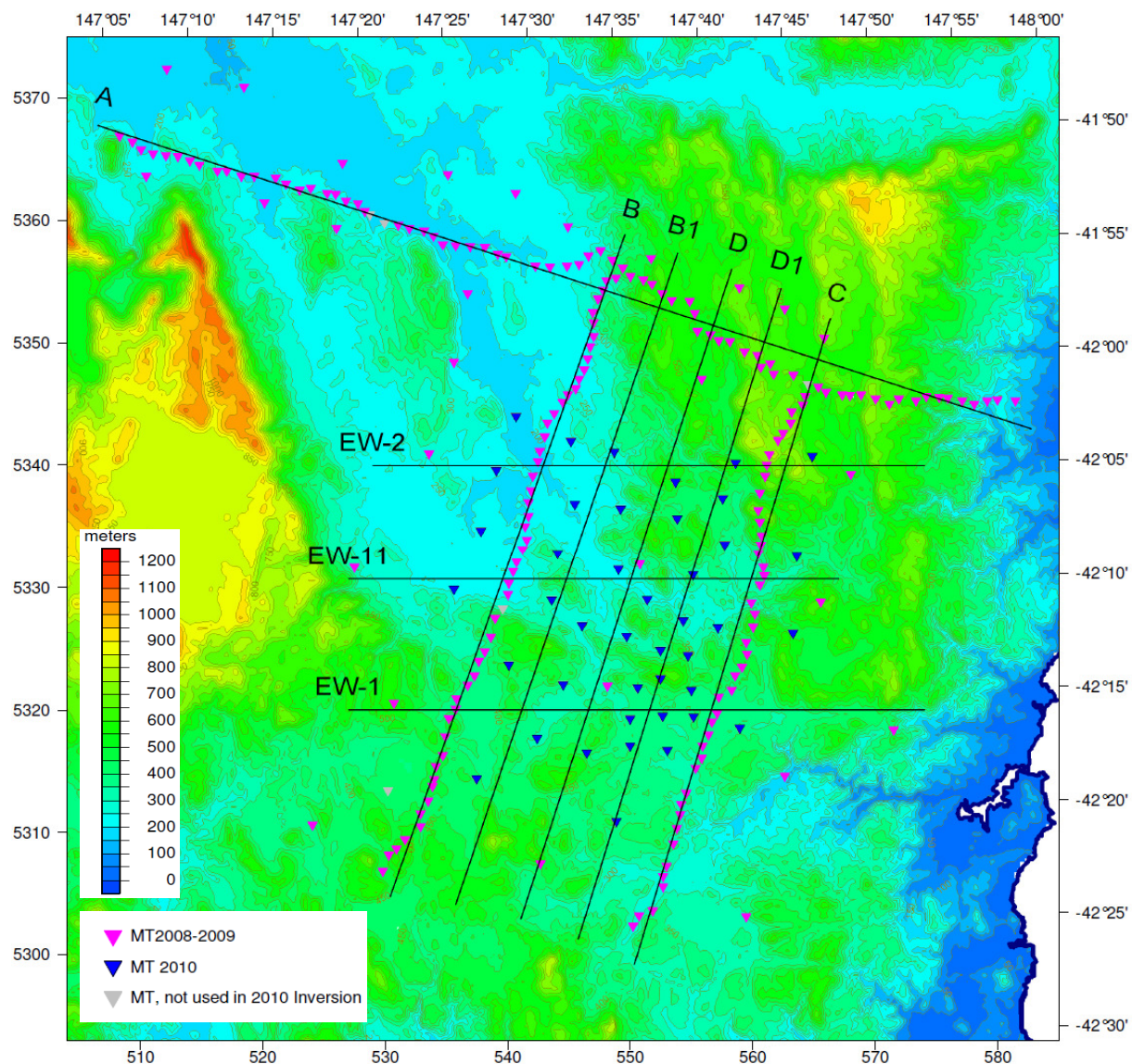


Figure 2. MT station and profile locations on topographic base map. Sites included in the 2010 3D MT inversion are marked in color.

The database created for the analysis of this data set uses the WGS84 coordinate system, as described below; all maps presented as well as the 3D modelling are referenced to this system.

Metric Coordinates:	Projection:	Transverse Mercator
	True Origin:	147°00' E, 0°00' S
	Coordinates at Origin:	500,000m E, 0m N
	Datum:	WGS84
Geographic Coordinates:	Spheroid:	WGS84
	Datum:	WGS84
	Spheroid:	WGS84
Elevation	Orthometric:	Extracted from 90m DEM in meters relative to mean sea level

2 DATA CHARACTERISTICS

MT data impedance and tipper parameter plots are presented in the next section. Example soundings are shown in Figure 3.

Data have been edited to mask noisier segments. A smooth curve, computed from the D+ function (Beamish and Travassos, 1992) is fitted to each component. Data which are geophysically plausible should lie close to this curve.

Acquisition Contractor:	Moombarriga Geoscience (all three projects).
Year of acquisition /	2008 / 43 (STLnnn)
Number of MT sites (IDs):	2009 / 158 (EWAAnnn / EWO[A/B]nn / NS[A/B]nnn / NSO[A/B/C]nn) 2010 / 43 (SITEnn)
Total Number of MT sites:	244
Area covered:	70km(EW) x 70km (NS)
Site spacing:	1 km – inline along profiles 2-3 km in the central part, between lines
Instrumentation	
Data loggers:	Phoenix MTU-5A
Magnetic sensors:	Phoenix MTC50
Frequency range:	300Hz – 0.0003Hz
Data Quality:	Generally good. Magnetic tipper data only available at about 50% of the sites.

The frequency range covered by the MT soundings of all three data sets is from 300Hz to over one thousand seconds in the best cases. Overall data quality is good, and there is no significant difference in quality between the 2010 and the 2008-9 impedance data sets.

2.1 Sounding Curves

Careful data editing by masking poorer data sections was performed prior to 3D inversion (illustrated in Figure 3). The masking on the 2008-9 data for the 2009 3D inversion was maintained for the new resistivity modeling done here.

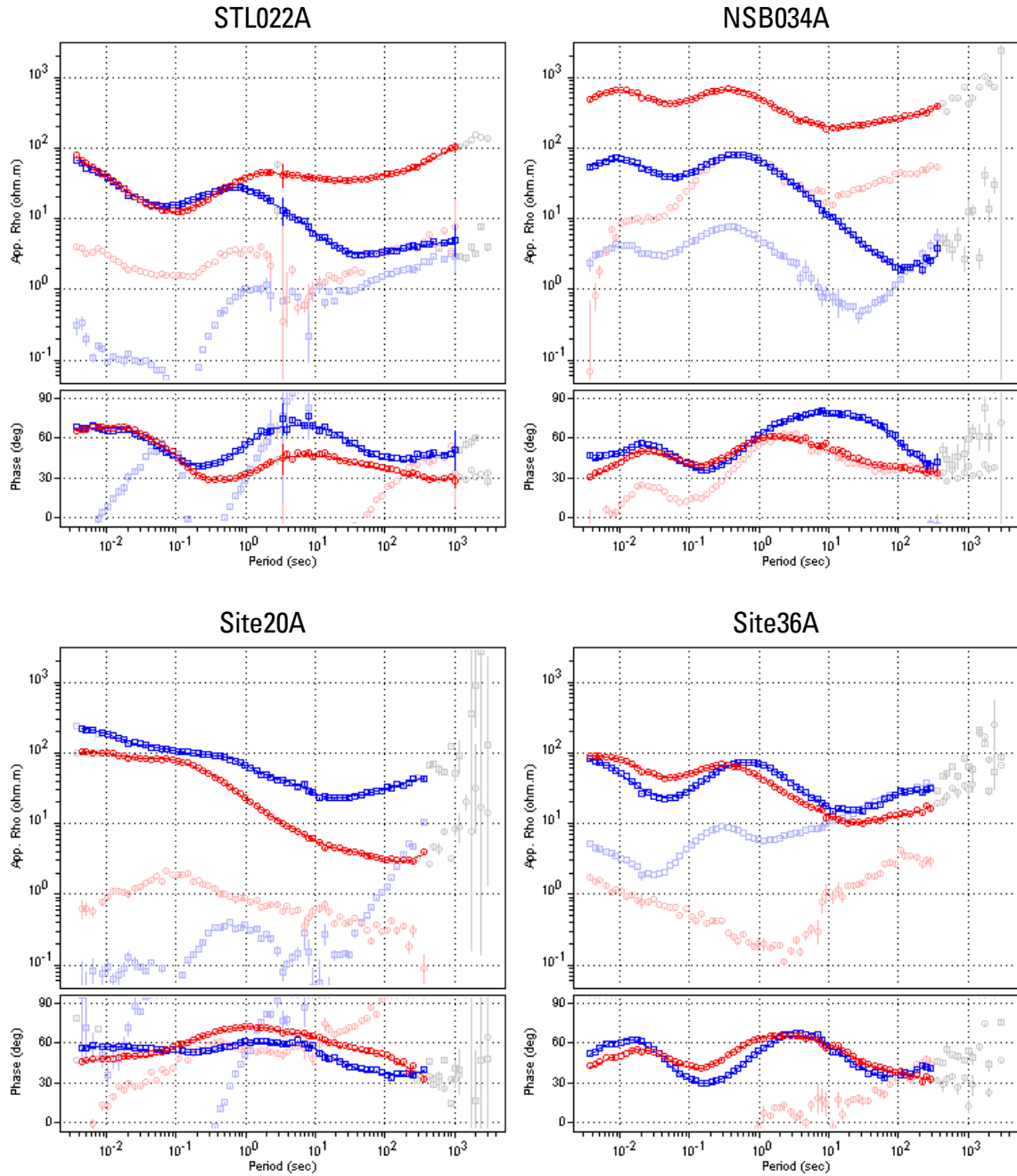


Figure 3. Example soundings STL022A and NSB034A from the 2008-2009 data set (upper panel) and Site20A and Site36A from the 2010 data set (lower panel). Data are rotated to N106°E, the rotation angle for the 3D modelling. Off-diagonal components xy (red) and yx (blue) are displayed in bold colors, on-diagonal tensor elements are in faint colours (xx and yy), and masked data in gray.

Static shift effects in apparent resistivity (i.e. the impedance amplitudes) are significant as discussed in the 2009 report, and evident from the example shown above (site NSB034A). Explicit inversion for static shift factors was therefore enabled in the 3D inversion calculations (see Section 3).

Magnetic tipper data were included in the 2010 inversion as done in the 2009 analysis. 25 of the 43 sites from the 2010 data set were found to have usable tipper information. At 17 sites noisy but systematic tipper data curves were found, with laterally very consistent values (see Figure 4). These data were judged to be unreliable and are not included in the last inversions. The

influence of their inclusion however was found to be small, however, given the high error bars and subsequent downweighting by the inversion. According to the contractor this is related to the application of a wrong calibration file at a number of sites where there was physically no vertical coil connected.

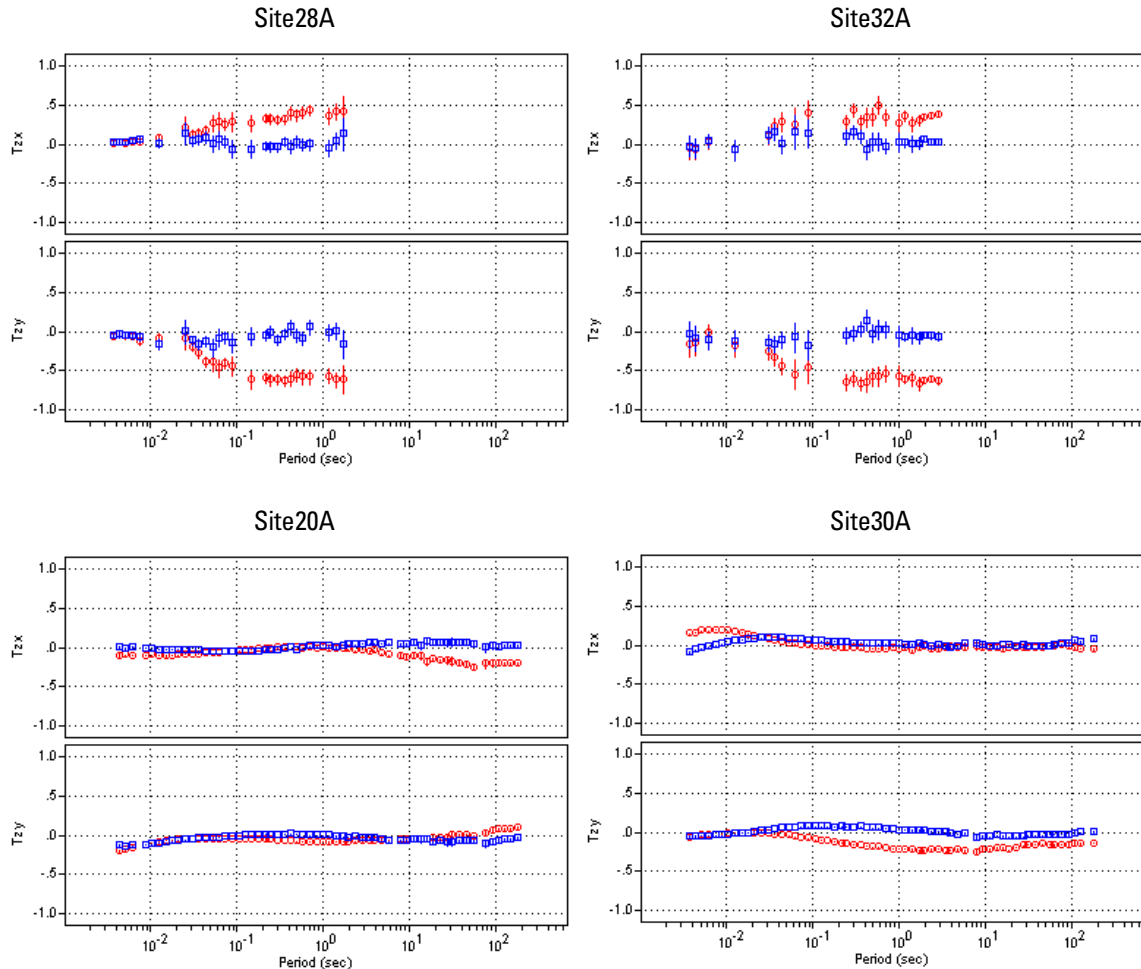


Figure 4. Example tipper curves of the 2010 data set: Site28A, Site32A (top), and Site20A, Site30A (bottom), after initial data masking (Geosystem). Real parts are shown in red, imaginary in blue.

2.2 Parameter Maps

Apparent resistivity maps are not presented here due to the prevalent static distortion effects described above. These are usually not present or much reduced in the impedance phases. Gridded impedance phase invariants are displayed in Figure 5, representing updated displays of the 2009 modeling report versions.

The main identifiable structure from these data plots have been discussed before: in the north-eastern section, high phase values at highest frequencies (here: 100Hz) relate to a continuous conductor at relatively shallow depth. In the same area, at one decade lower frequencies, a conductive to resistive transition is indicated with increasing depth (10Hz). At intermediate frequencies (1Hz), a NW-SE conductive band at greater depth is marked by a high phase ridge, in accordance with tipper information at longer periods. Also at longer periods, high phases in the southernmost section hint at very deep conductors in this area.

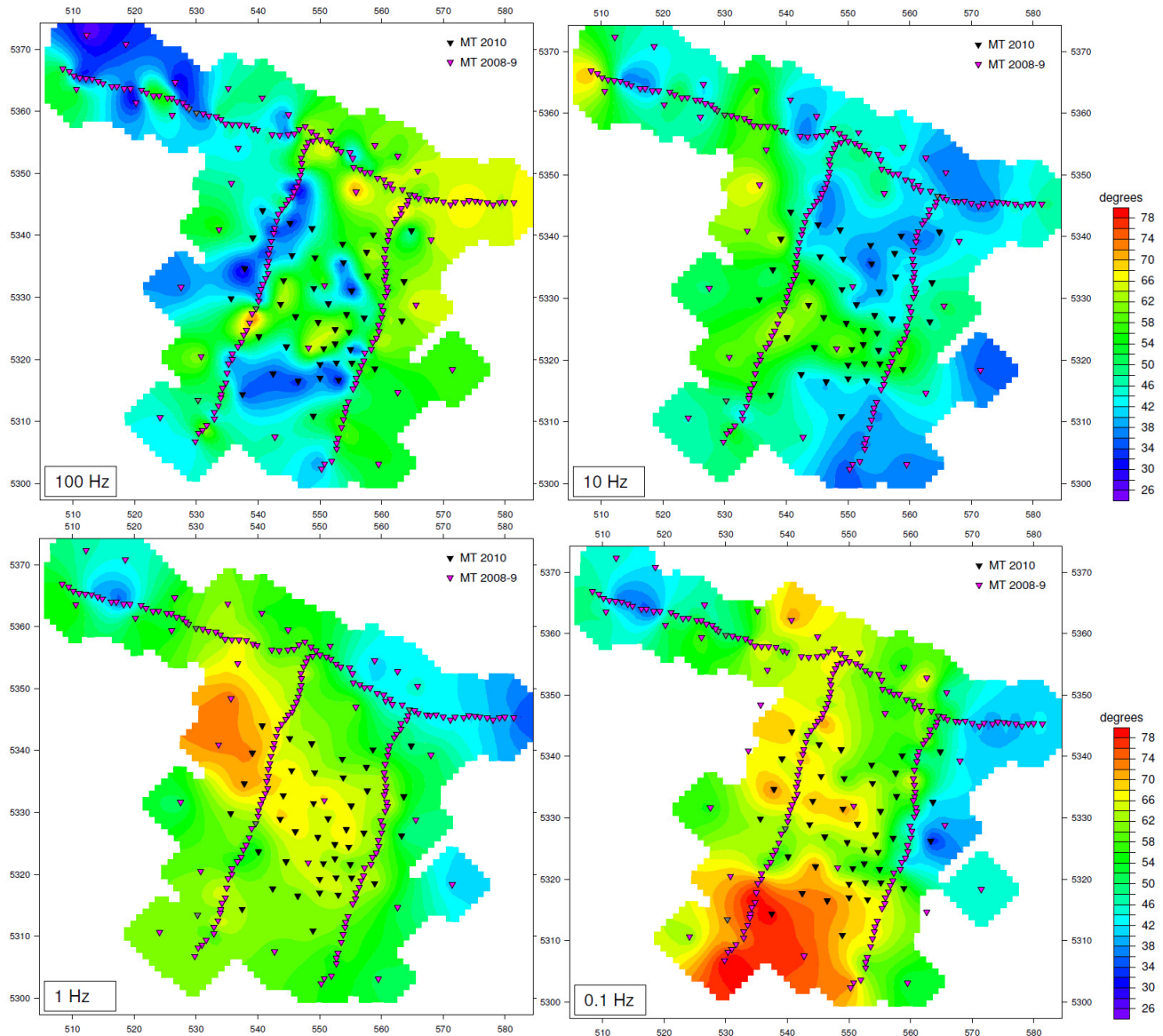


Figure 5. Impedance phase Invariant for the combined 2008-9 and 2010 MT data set at frequencies 100Hz, 10Hz, 1Hz, and 0.1Hz.

With respect to the 2008-9 data set, the impedance maps highlight more east-west oriented structure perpendicular to the lines B & C: at high frequency (100Hz), a zone of low phases is marked in the southern section between the lines, and elevated phases just north of this zone. At low frequencies (0.1Hz), the boundary to the southern zone of high phase – related to low resistivity at greater depth – is more sharply resolved, also with a ~W-E trend. North of this zone, a second ridge of high phase is marked between lines B & C.

2.3 Induction Vectors

Slightly over half of the MT sites contain magnetic tipper data – i.e. transfer functions between vertical and horizontal magnetic field components. In Figure 6 real parts of these vectors are displayed for frequencies 10Hz, 1Hz, 0.1Hz and 0.01Hz in the reverse convention i.e. pointing towards conductors.

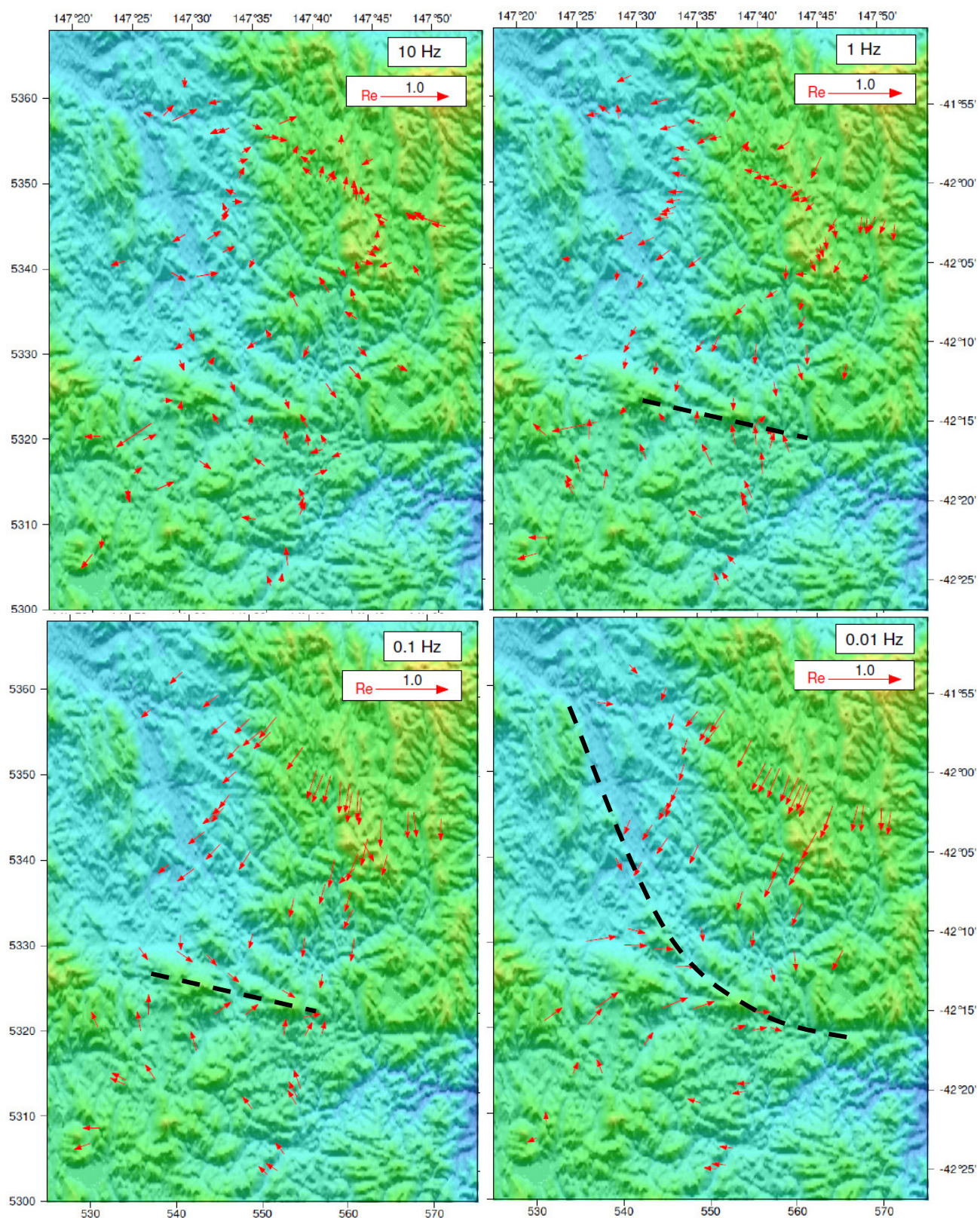


Figure 6. Real induction vectors for 10Hz, 1Hz, 0.1Hz and 0.01Hz (top left to right bottom). Arrows are plotted in the convention pointing *towards* conductors. Black dashed lines show how high conductivity is indicated at major fault locations.

3 MT MODELING – 3D INVERSION

Full Tensor MT 3D inversion modelling, including topography and bathymetry, was carried out using the code described by Mackie and Madden (1993) subsequently developed and implemented by Geosystem. The regularization operator produces a smoothly varying resistivity volume, consistent with the gradual resistivity changes expected within a geothermal system. A summary of the 3D modelling technique is given in Appendix B, and the complete set of inversion parameters used is summarized in Appendix C.

The parameters listed below are taken from the preferred inversion based on an 800m grid, and referred to as model #5 (see Appendix C).

The inversion on the fine mesh (1,341k cells) was run on a Linux cluster of 308 cores (154 CPUs) within 64 hours for 50 iterations.

3.1 Mesh Dimensions

The dimensions of the mesh (number of cells) need to be designed such that a result with sufficient accuracy can be achieved in reasonable computation time, while considering the data distribution and target dimension.

Mesh orientation:	N106°E (E16°S in mesh system)
Topography:	90m DEM from SRTM.
Topographic variation:	~0-1000m msl
Bathymetric variation:	-150m msl at 50km; -4000m msl at 120km
Minimum cell dimension (at topography):	800m x 800m x 30m
Deep vertical cell dimension (-600m to -4,500m msl)	100m
Number of cells in x, y, z direction:	121 x 99 x 112
Total number of cells:	1,341,648

Padding (to avoid model boundary issues):

Number of horizontal padding cells:	10 per direction
Lateral, vertical augmentation per cell:	50% and 20%, respectively
Total mesh dimension:	353 km x 335 km x 74 km

To avoid computational errors the mesh was checked for isolated cells above the topography before running the models.

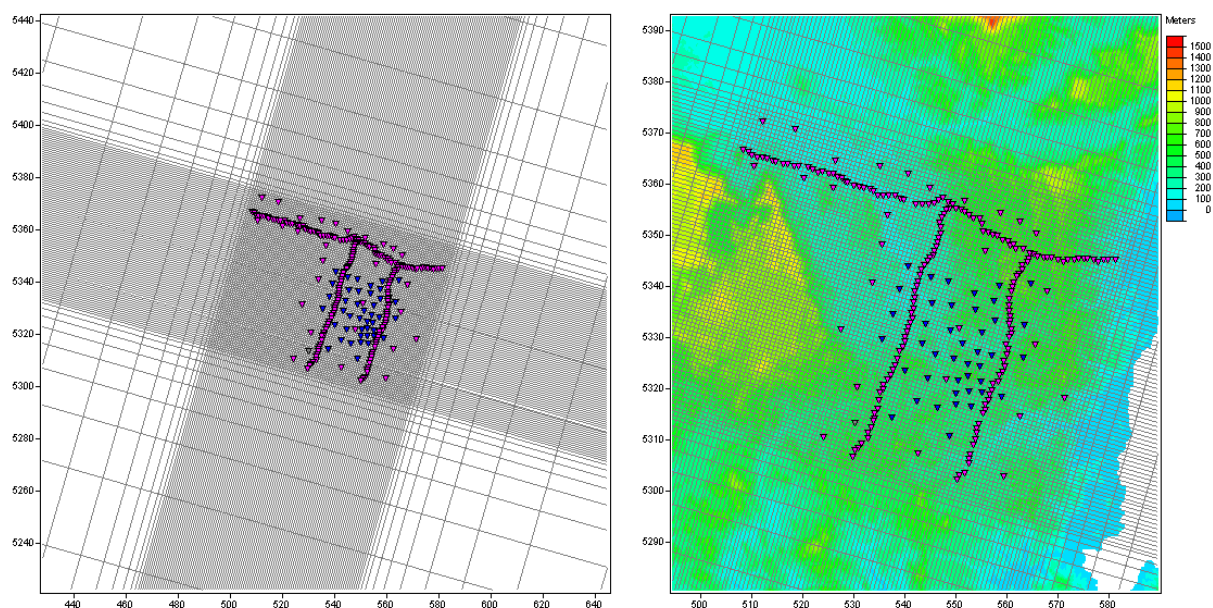


Figure 7. Plan views of full 3D model meshes (LHS) and fine mesh centred on MT station locations (RHS). Background grid is topography (SRTM DEM).

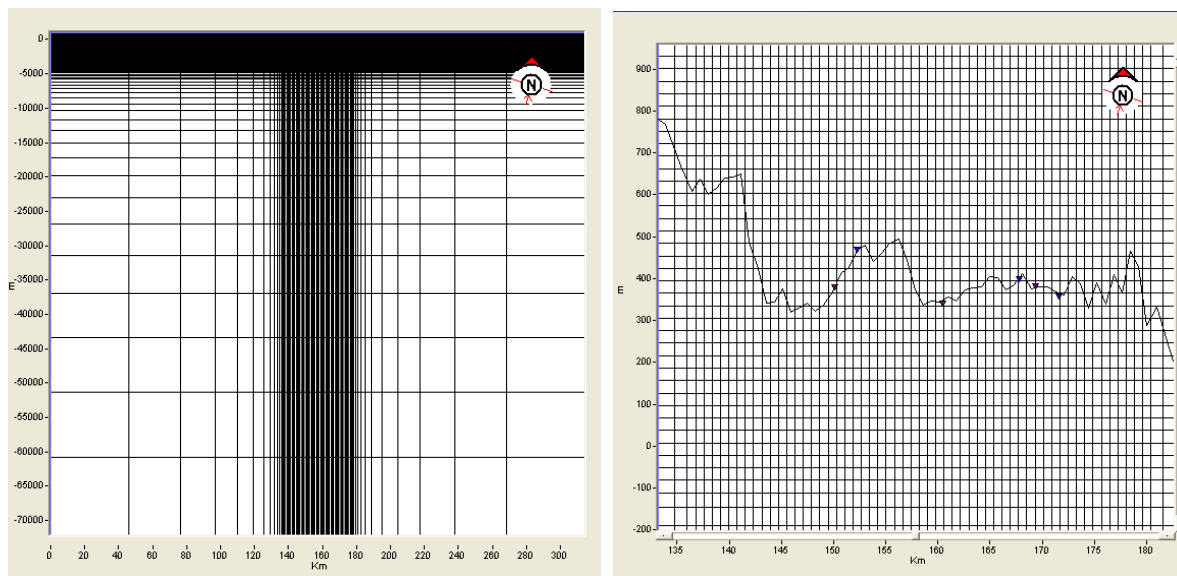


Figure 8. Section views of full and core 3D model mesh (LHS, RHS), showing also the intersection with the elevation grid (RHS).

3.2 Data Input

Number of MT sites included:

238

6 sites were excluded, due to low data quality (STL027A, EWA023A, EWA024A, NSA0321A, Site03A), or co-location with another site (EWA013A).

Full tensor impedances (complex):

In Zxy, Zyx

Zxx, Zyy

Magnetic tipper data (complex):

Tzx, Tzy

Tensor / Vector rotation angle

N106°E (in line with the 3D mesh)

Number of frequencies:	21
Frequency range:	0.003 – 300Hz
Frequencies per decade:	4
Total number of data points:	43,617

3.3 Inversion Parameters

Code version:	1.1.6
Regularization:	uniform grid laplacian
Tau:	3
= trade-off parameter between data fit and model structure: low numbers result in higher data fit (lower RMS) and more model structure.	(successively reduced from 10 with inversion re-starts)
Number of iterations:	30 (cumulative: 50)
Error floors:	3% (ln Zxy/yx) 20% (Zxx/yy) 0.02 (Tzx/Tzy)
Static shift factor inversion:	Inverted variance: 10% damping: 100 (after 1000 in #4).

3.4 Data Fit

The overall data fit of the 3D inversion algorithm is quantified by the error measure

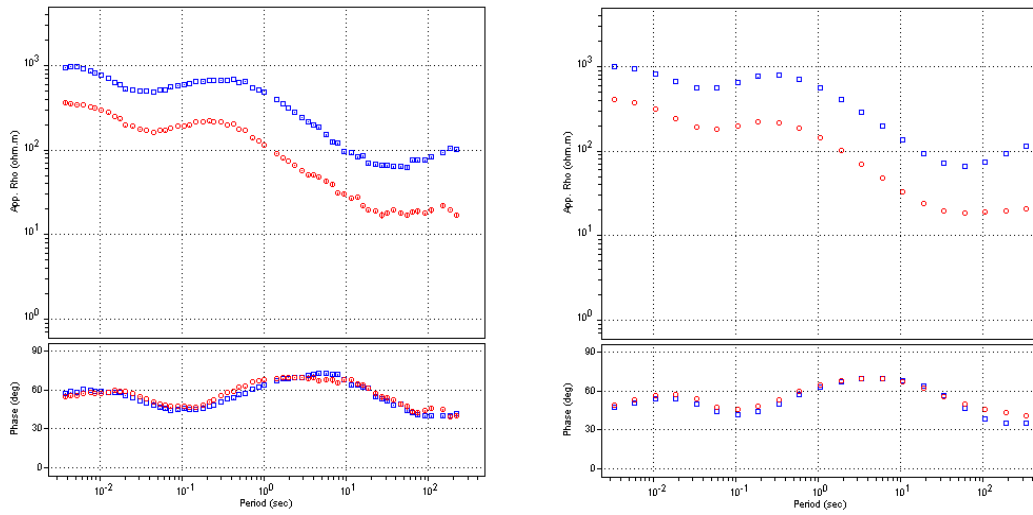
$$\text{RMS} = \sqrt{\frac{1}{npts} \sum \frac{(obs - pred)^2}{var}},$$

with *obs* and *pred* denoting observed and predicted data responses. *Npts* is the number of data points, and *var* refers to the variance or data error of each datum. From this, it is clear that decreasing the variance (i.e. the error floors) has the effect of increasing the RMS misfit, and vice-versa. The RMS error for inversion #5 is:

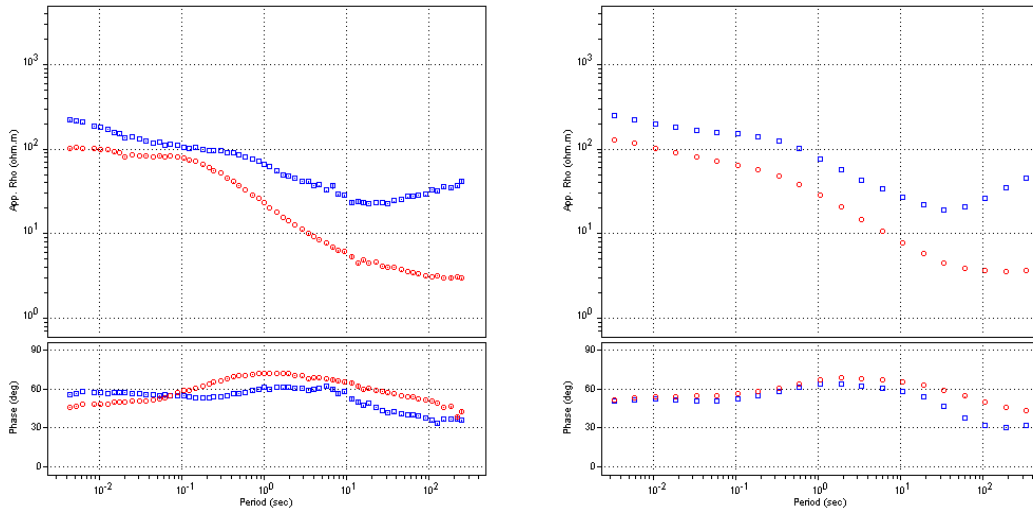
RMS:	2.525
------	-------

The RMS misfits for each sounding, together with other model and response files are provided on CD in Appendix D. Examples of computed vs. observed responses are shown in Figure 9.

NSA014A, RMS=1.45



NSB044A, RMS=2.99



SITE20A, RMS=2.27

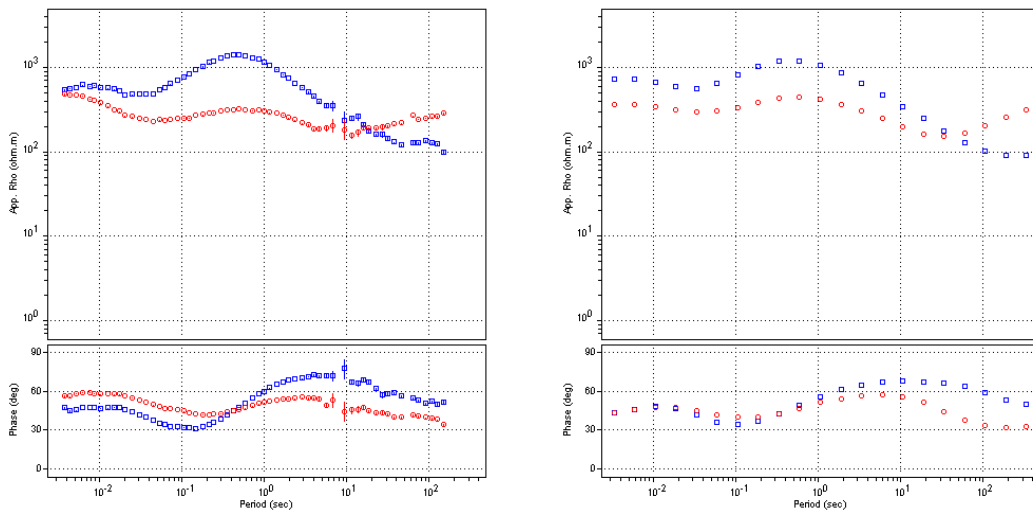


Figure 9. Example MT soundings NSA014A, SITE20A and NSB044A show fit between observed (LHS) and calculated 3D model response (RHS). Data are rotated in 3D mesh direction. Note the final resistivity model reproduces the static shifts inherent in the MT data at NSA014A, both through inclusion of near-surface structure and direct static shift factors.

3.5 Modeling Results

Resistivity depth maps from the inversion model #5 are presented for elevations -500, -1000, -1500, -2000, -2500 and -3000 meters in Figure 10. Cross-sections through the 2009 and 2010 models along the main profiles A/B/C as well as additional lines are presented in Figure 12 to Figure 17. For the main lines, a comparison between 2009 and 2010 inversion results is presented.

As in the 2009 inversions, a NW-SE high conductivity band is modelled, linked to fault zones and to the TCZ (Tamar Conductivity Zone), somewhat compartmentalized. The addition of new sites allows for better imaging of an E-W oriented anomaly and discontinuity in the southern area, roughly in line with profile EW-1. Both the NS-SE and the E-W oriented anomalies are supported by the orientation of induction vectors from magnetic transfer functions only (Figure 6).

Note that very deep structure (<-4km msl) is not very well resolved and should not be over-interpreted.

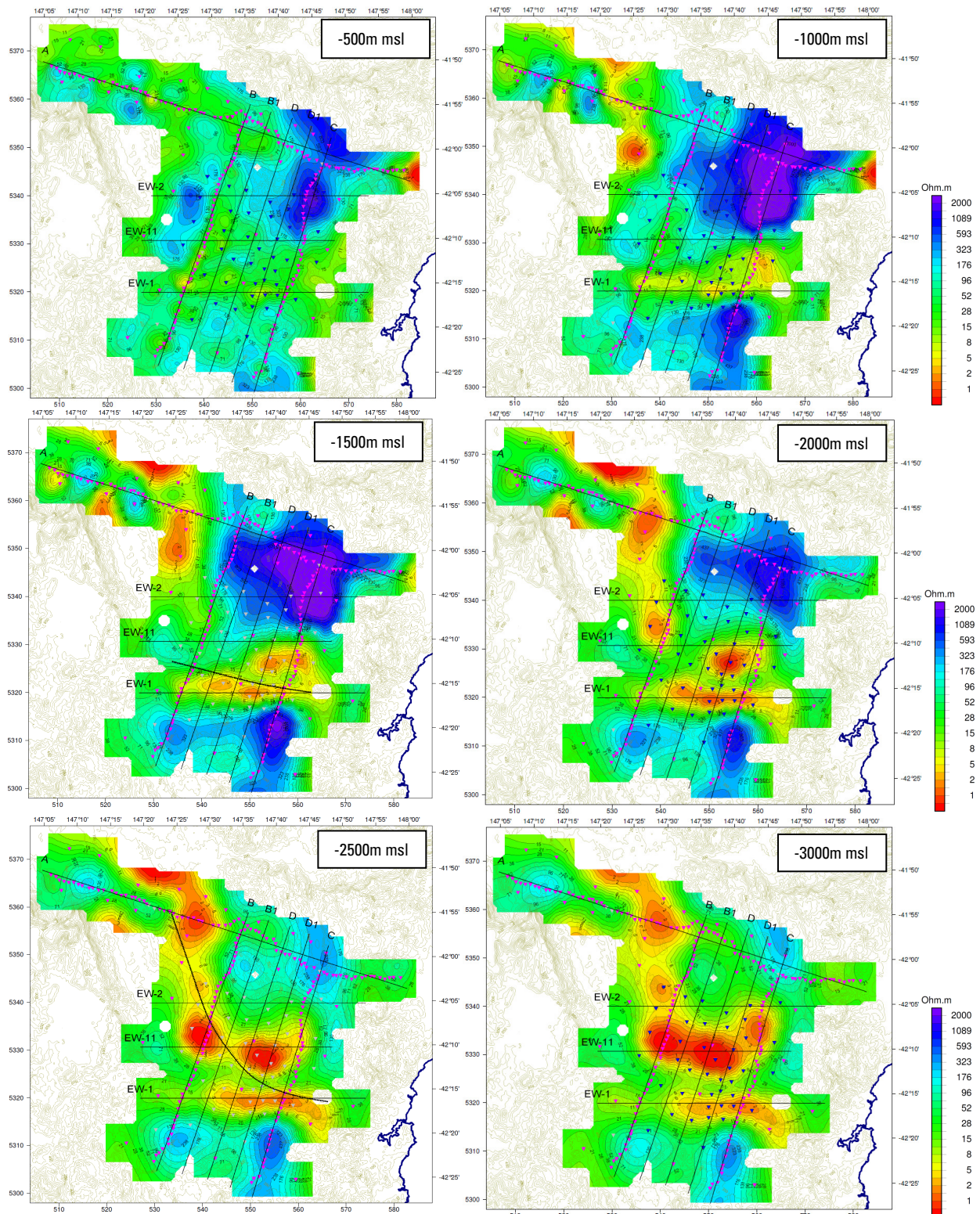


Figure 10. Resistivity depth maps from -500 to -3000m msl from the 2010 3D MT inversion (from top left to bottom right). Blue sites are from the new 2010 data set. The dashed black lines at elevations -1500m and -2500m msl mark the high conductivity trends inferred from induction vector maps at 0.1Hz and 0.01Hz, respectively (, Figure 6).

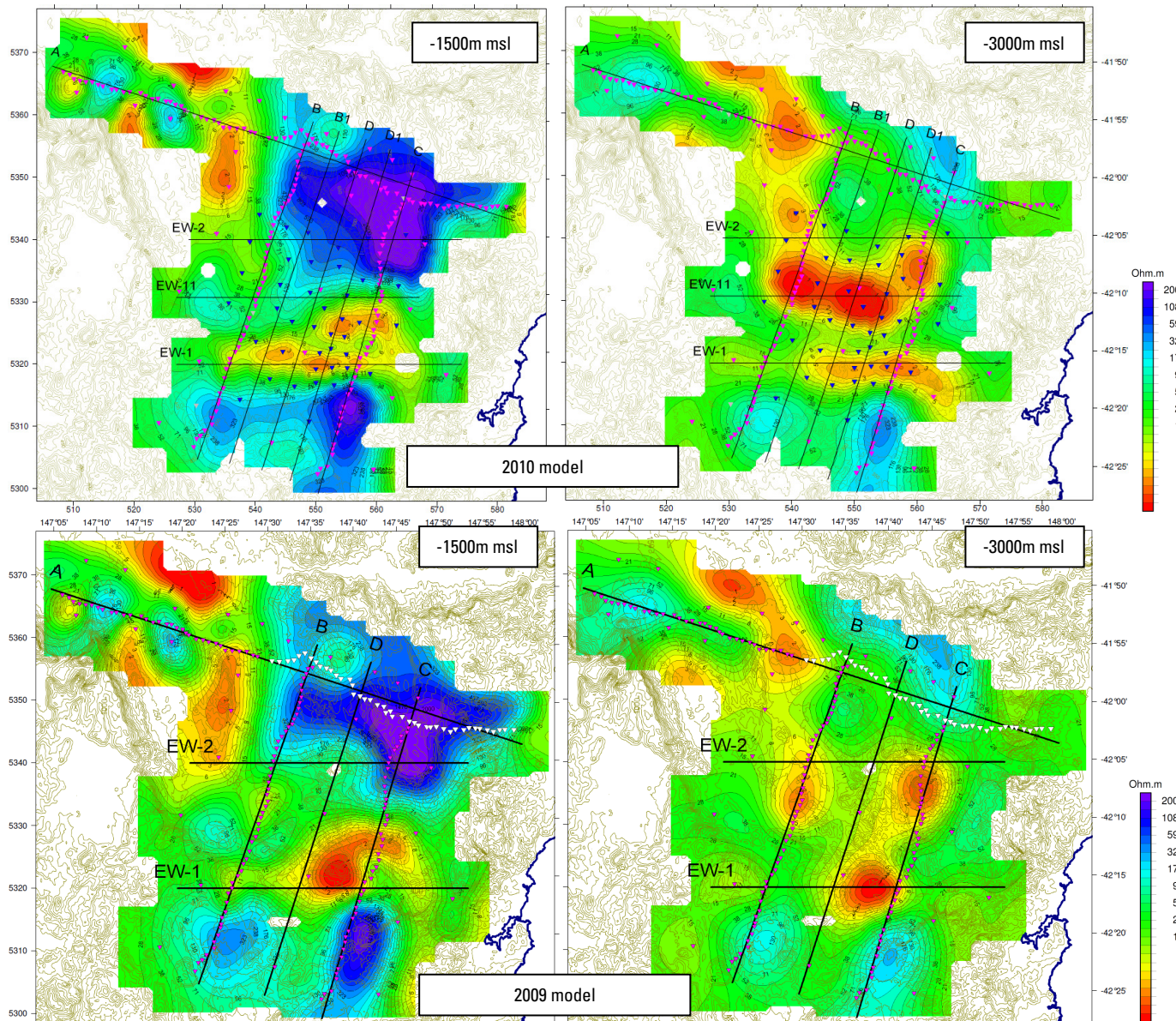


Figure 11. Resistivity depth maps at -1500 and -3000m msl from 3D MT inversion compared to the 2009 results (bottom). Blue sites are from the new 2010 data set.

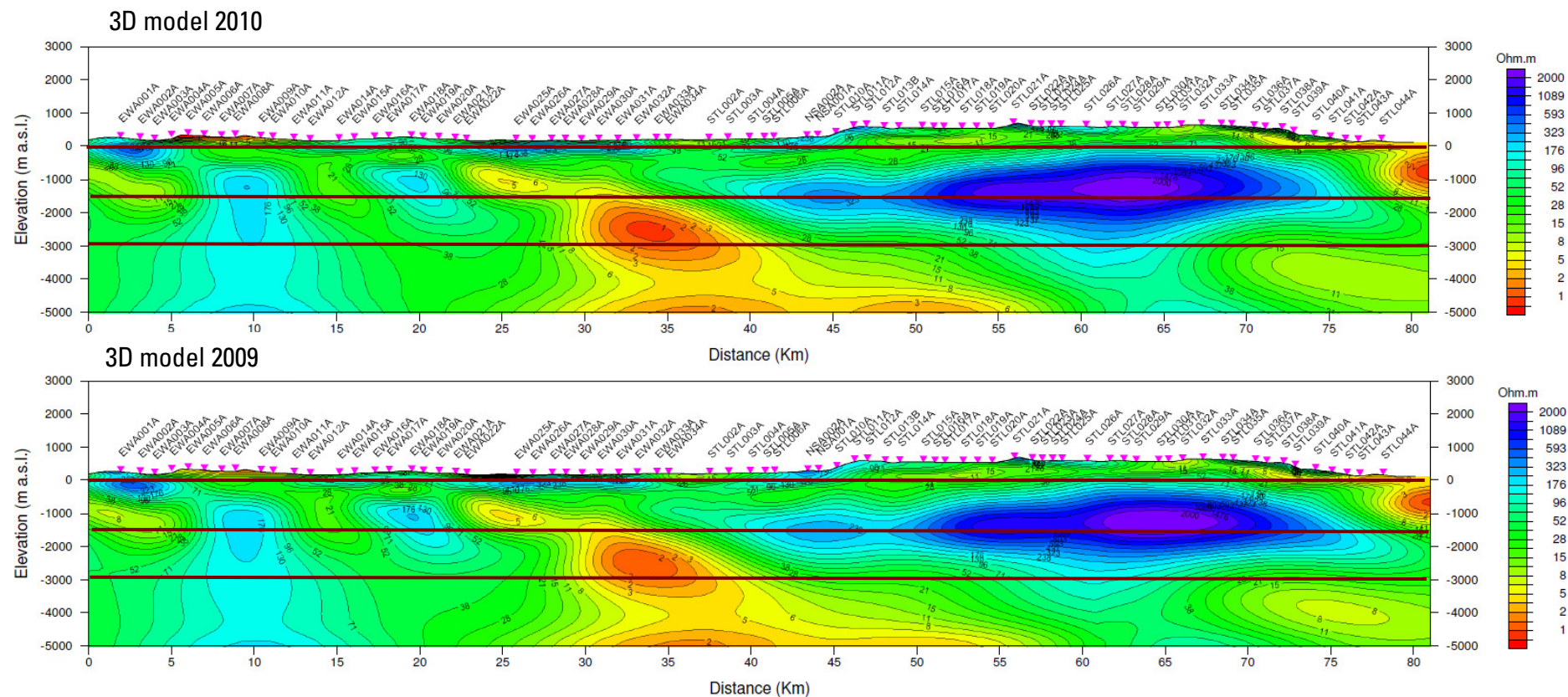
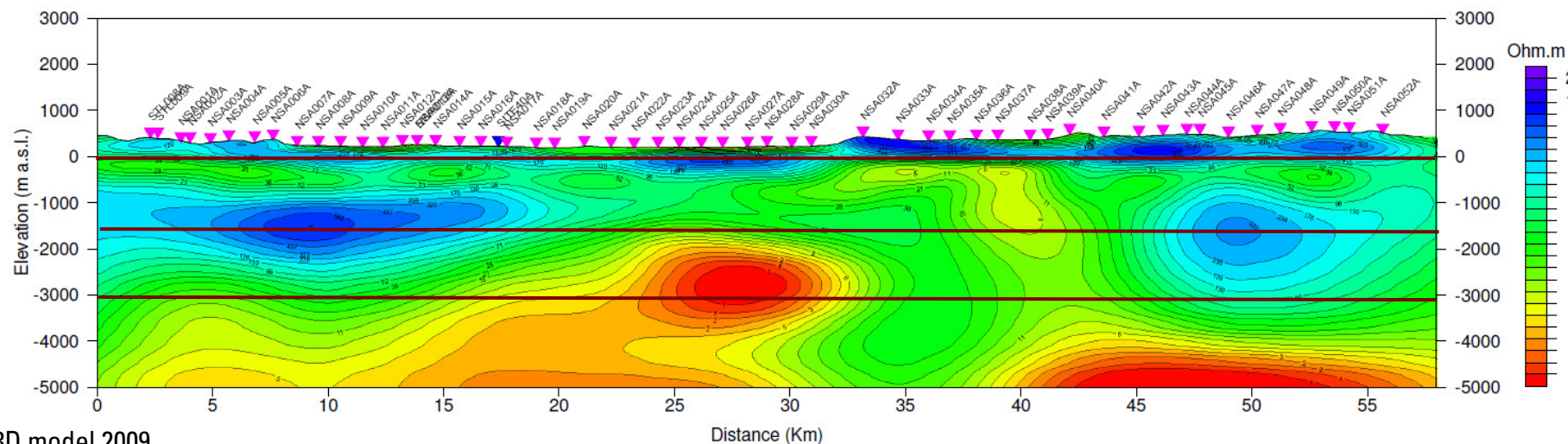


Figure 12. Cross section along profile “A” through the 3D resistivity model (NW to SE, top), compared to the 2009 inversion result (bottom).

3D model 2010



3D model 2009

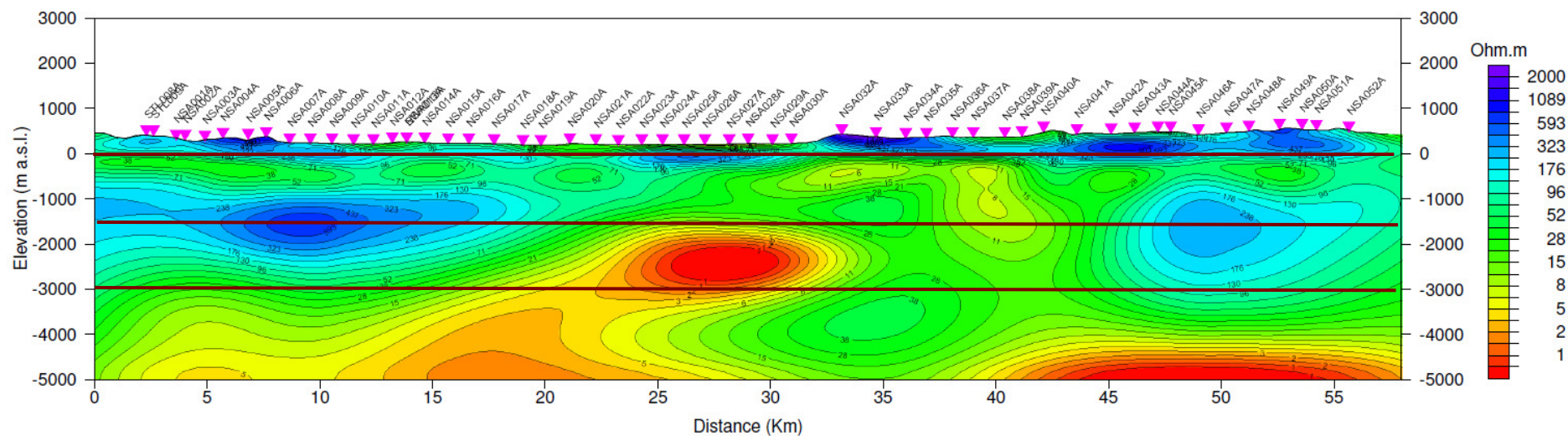
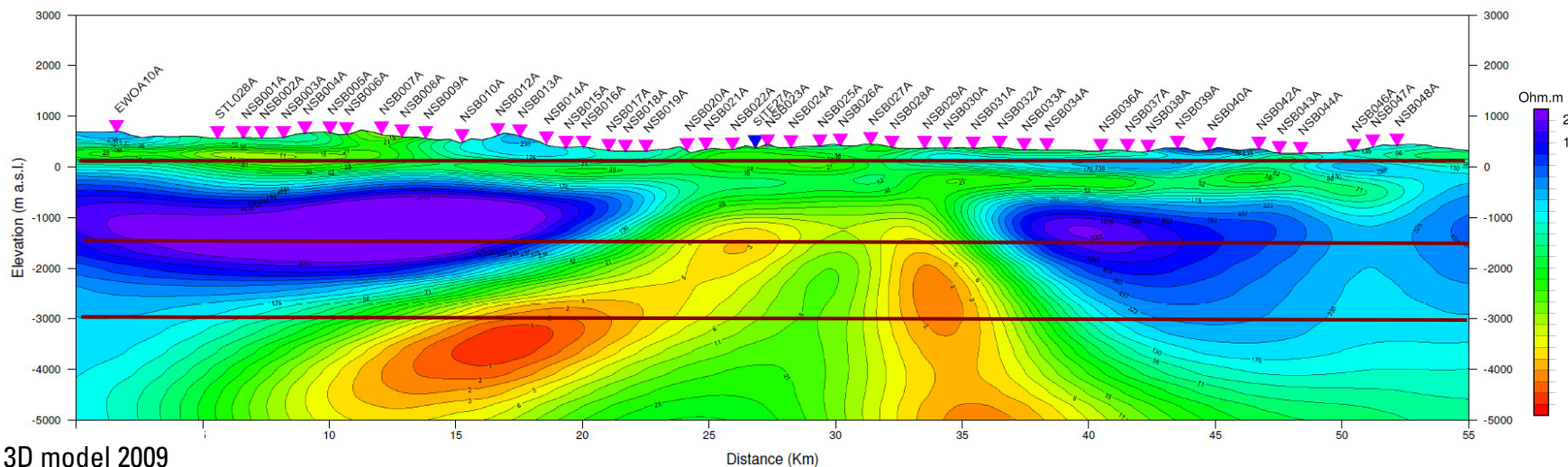


Figure 13. Cross section along profile "B" through the 3D resistivity model (NE to SW, top), compared to the 2009 inversion result (bottom).

3D model 2010



3D model 2009

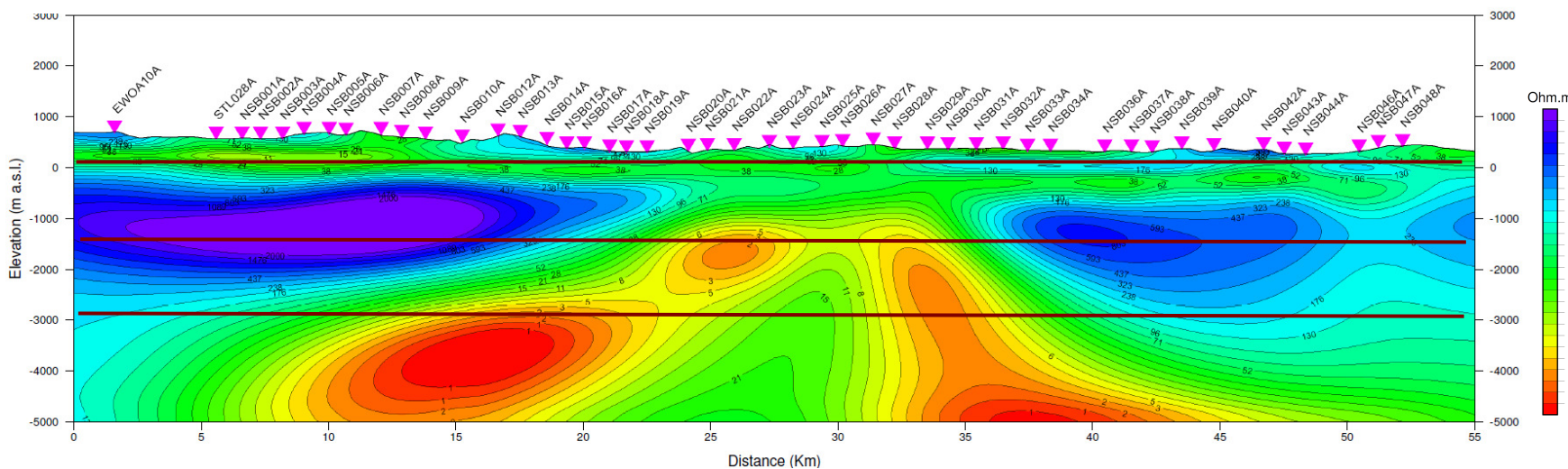


Figure 14. Cross section along profile "C" through the 3D resistivity model (NE to SW, top), compared to the 2009 inversion result (bottom).

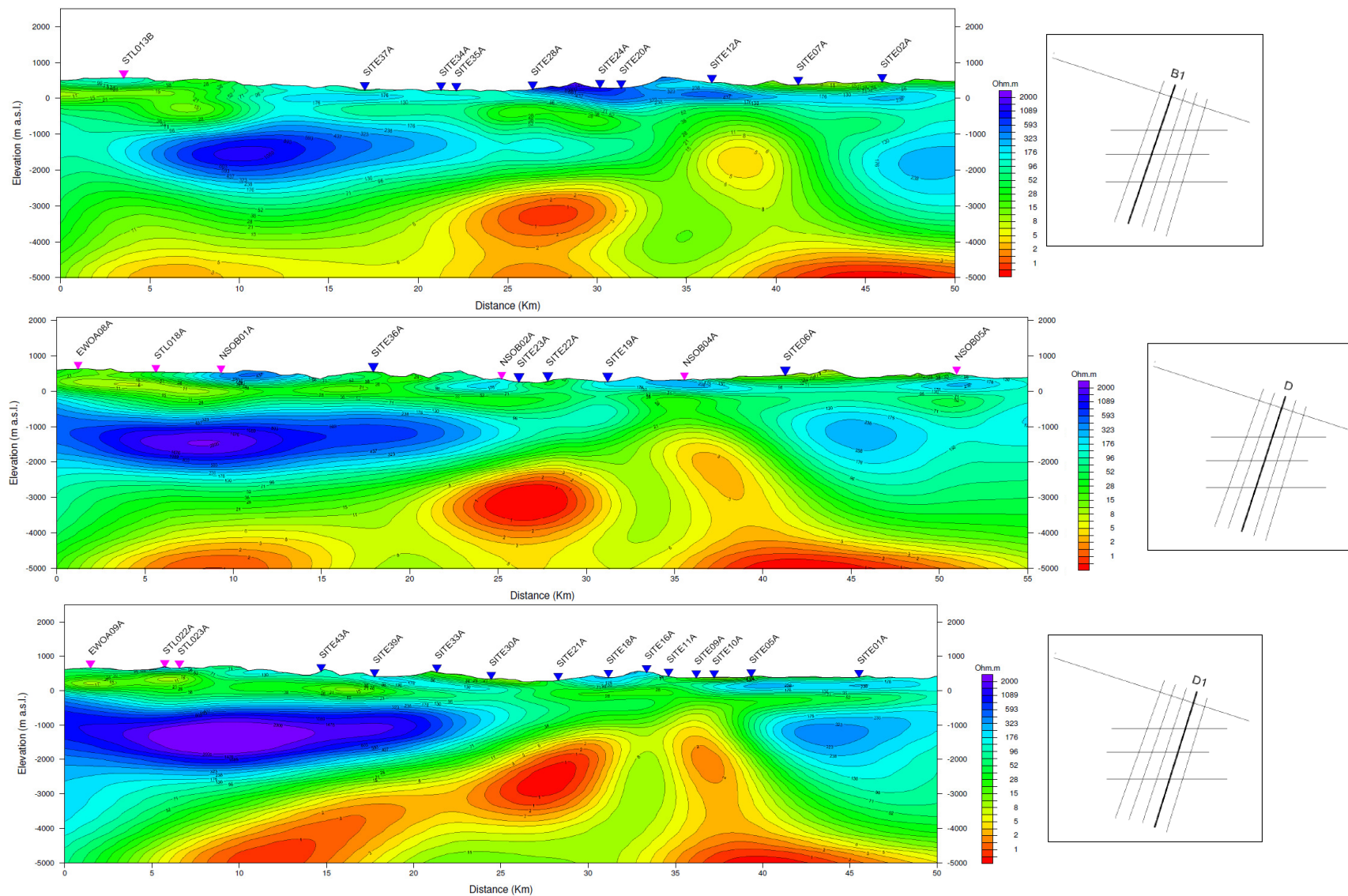
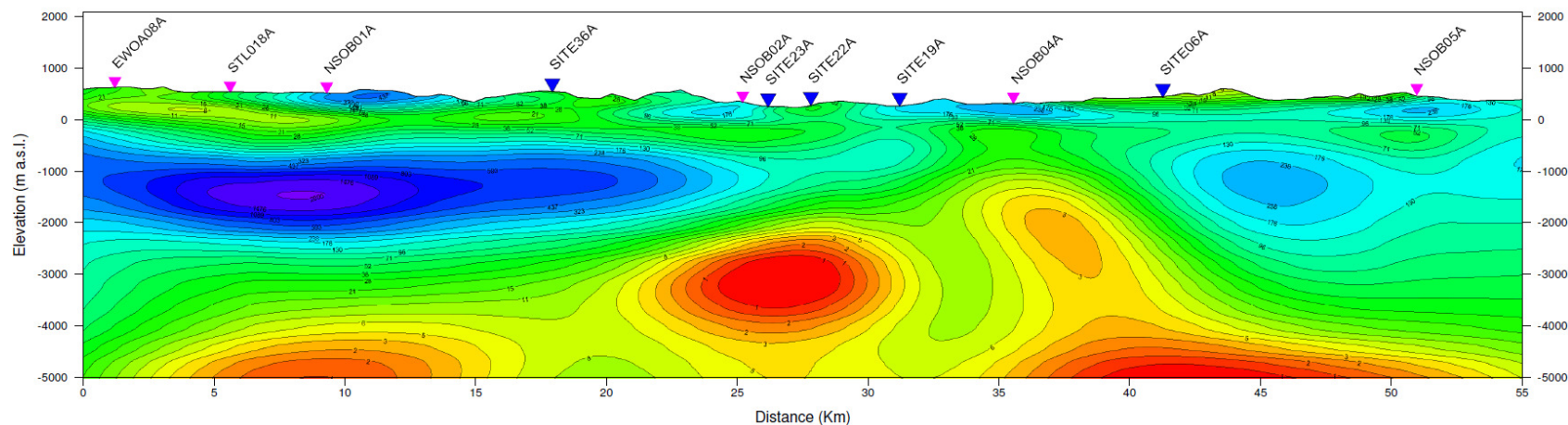


Figure 15. Cross section along profiles “B1”, “D” and “D1” through the 3D resistivity model (N is to the left). Blue sites are from the new 2010 data set.

3D model 2010:



3D model 2009:

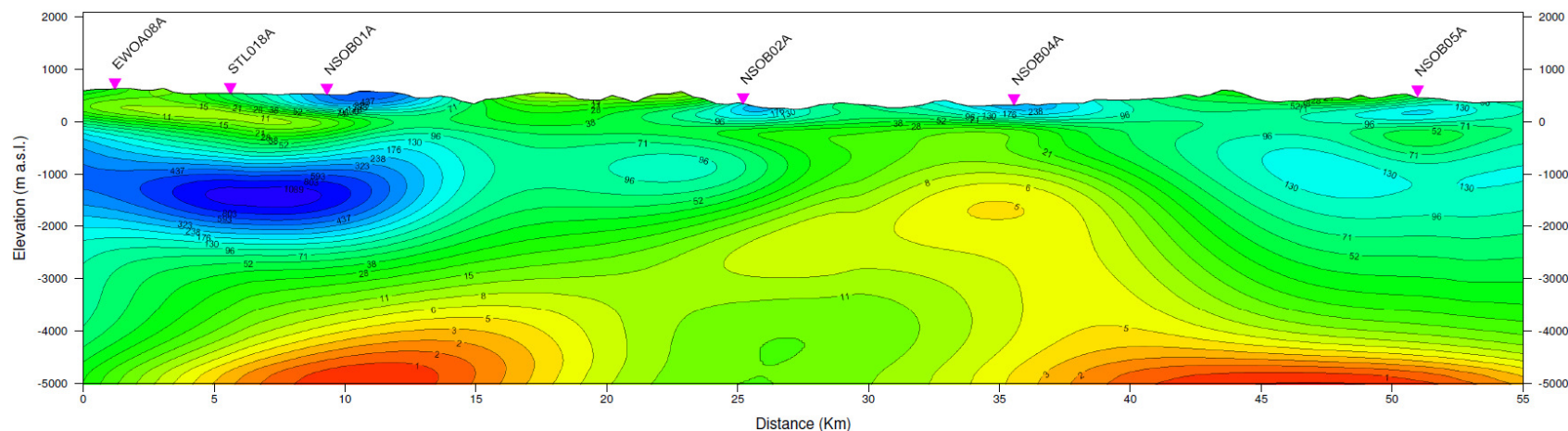


Figure 16. Cross section along profile “D” through the 3D resistivity model (NE to SW, top), compared to the 2009 inversion result (bottom). Blue sites are from the new 2010 data set.

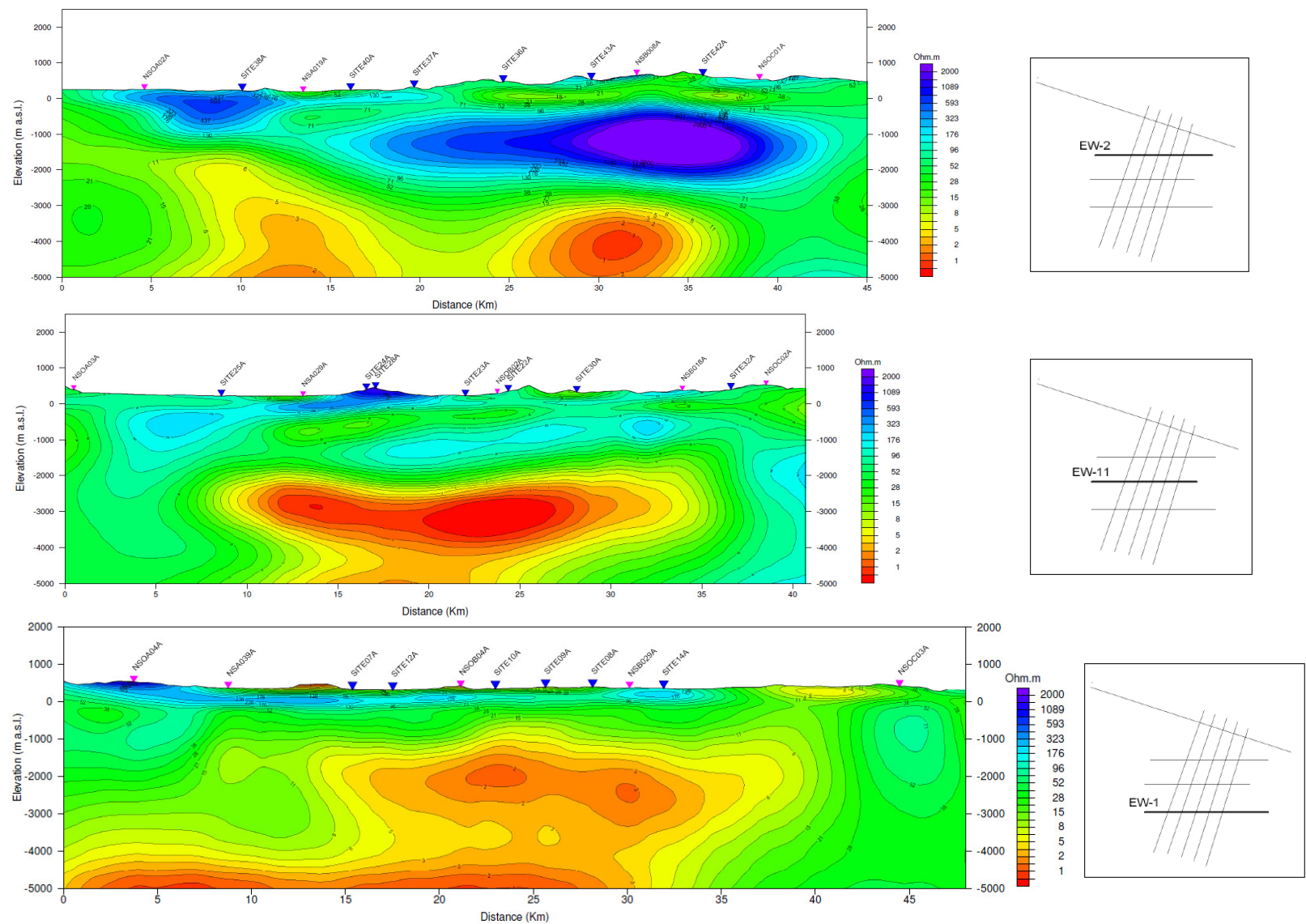
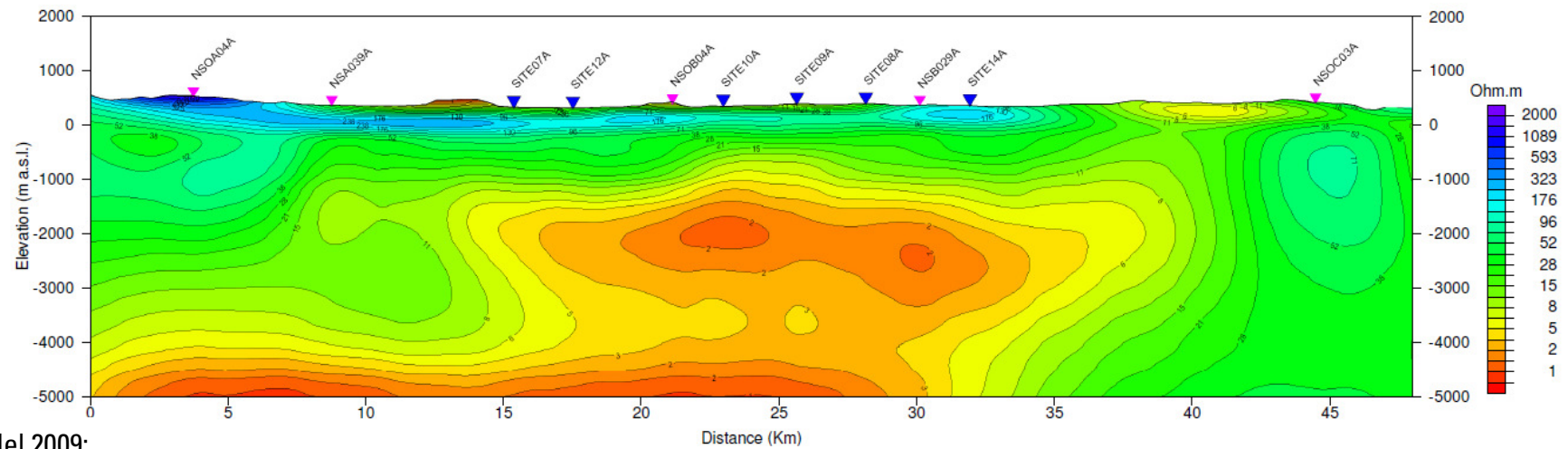


Figure 17. Cross-sections along profiles “EW-2”, “EW-11”, and “EW-1” (top to bottom) through the 3D resistivity model (W is to the left). Blue sites are from the new 2010 data set.

3D model 2010:



3D model 2009:

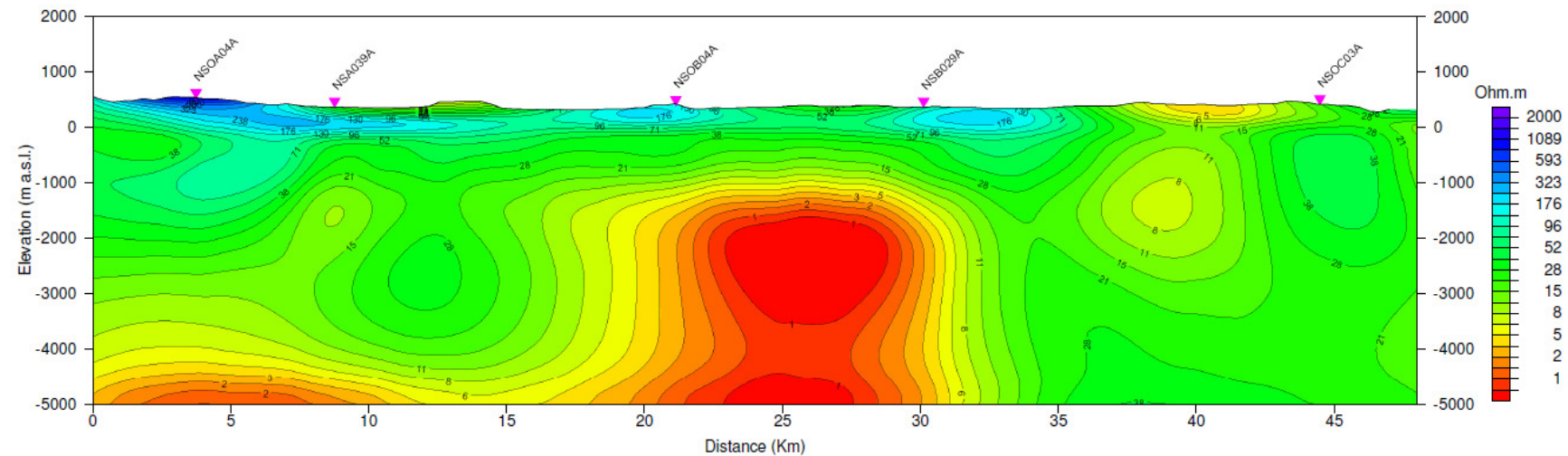


Figure 18. Cross section along profile “EW-1” through the 3D resistivity model (top), compared to the 2009 inversion result (bottom). Blue sites are from the new 2010 data

4 BIBLIOGRAPHY

- | | | |
|--|------|--|
| Andrieux, P. and Wightman, W. E. | 1984 | The so-called static corrections in magnetotelluric measurements, <i>54th Ann. Internat. Mtg: Soc. of Expl. Geophys., Session:EM1.1.</i> |
| Beamish, D., and Travassos, J. | 1992 | The use of D+ in Magnetotelluric interpretation: <i>J. Appl. Geophys</i> 29 , 1-19. |
| Cull, J.P. | 1991 | Heat Flow and Regional Geophysics in Australia, <i>in</i> Terrestrial Heat Flow and the Lithosphere Structure, Cermak, V. and Rybach, L. (Eds.), <i>Springer-Verlag</i> , 486-500. |
| deGroot-Hedlin, C., and Constable, S. | 1990 | Occam's inversion to generate smooth, two-dimensional models from magnetotelluric data, <i>Geophysics</i> , 55 , 1613-1624. |
| Fletcher, R. and Reeves, C.M. | 1959 | Function minimization by conjugate gradients, <i>Computer J.</i> , 7 , 149-154. |
| Geosystem | 2009 | Magnetotellagnetotelluric (MT) Data – 3D Inversion Modeling, Eastern Tasmania, Australia. Final Report prepared for KUTH Energy. |
| Mackie, R.L., and Madden, T.R. | 1993 | Three-dimensional magnetotelluric inversion using conjugate gradients: <i>Geophys. J. Int.</i> , 115 , 215-229 |
| Mackie, R.L., Rodi, W., and Watts, M.D. | 2001 | 3-D magnetotelluric inversion for resource exploration: paper PF3.3, <i>Extended Abstracts, Ann. Mtg. SEG</i> |
| Polak, E. | 1971 | Computational Methods in Optimization: A Unified Approach, Academic Press, New York. |
| Press, W.H., Teukolsky, S.A., Vetterling, W.T., and Flannery, B.P. | 1992 | Numerical Recipes in FORTRAN: The Art of Scientific Computing, Second Edition, Cambridge University Press. |
| Rodi, W., and Mackie, R.L. | 2001 | Nonlinear conjugate gradients algorithm for 2-D magnetotelluric inversion, <i>Geophysics</i> , 66 , 174-187. |
| Smith, J.T., and Booker, J.R. | 1991 | Rapid inversion of two- and three-dimensional magnetotelluric data, <i>J. Geophys. Res.</i> , 96 , 3905-3922. |
| Soyer, W., Hallinan, S., Mackie, R.L., and Cumming, W. | 2008 | Statics in Magnetotellurics - Shift or Model?, 70th EAGE Conf. & Exhibition, Rome, June 9-12, 2008, extended abstract D020. |
| Tikhonov, A.N., and Arsenin, V. Y. | 1977 | Solutions of Ill-Posed Problems, V.H. and Sons: Washington, D.C. |
| Vozoff, K. | 1991 | The magnetotelluric method <i>in</i> Electromagnetic <i>Methods in Applied Geophysics</i> , Vol2B 641-711, pub. SEG. |
| Wannamaker, P.E., Hohmann, G.W., and Ward, S.H. | 1984 | Magnetotelluric responses of three-dimensional bodies in layered earths, <i>Geophysics</i> , 49 , p. 1517-1533. |
| Zhdanov, M.S. | 2002 | Geophysical inverse theory and regularization problems: Elsevier, <i>Methods in Geophysics</i> 36. |

APPENDIX A GLOSSARY

1D	The earth is assumed to be made up of homogeneous horizontal layers
2D	Geology is assumed to be uniform along strike, but varies in the dip direction.
3D	Geology varies in all 3 directions (x, y, and z)
bgl	Below ground level
bsl (asl)	Below sea level (above sea level)
Coils	Sensors used to measure time-varying magnetic fields
Conductance	For a layer, product of layer thickness \times conductivity (Siemens, S). See also Total Conductance, below.
Conductivity	1/resistivity (in S/m).
Contact resistance	Resistance of the electrode pot relative to a ground, measured in Ω .
E-line	Cable used to measure the electric field
EM	Electromagnetic
E_x and E_y	Electric field strengths, in units of mV/km, measured in the x and y directions respectively.
f	frequency, in Hertz (Hz)
H_x , H_y , and H_z	Magnetic field strengths, in units of nT, measured in the x, y, and z directions (z positive upwards).
Induction arrow	Real part of the vector $\begin{bmatrix} T_x & T_y \end{bmatrix}$, illustrating the relation between the vertical and horizontal magnetic field components from $H_z = T_x H_x + T_y H_y$, plotted to show direction towards an assumed 2D line-source (i.e. towards the conductor in the so-called reversed convention).
LaToracca skew angle	$=90^\circ - (\theta_{EH})$, where θ_{EH} is the angle between the major axes of the E and H polarization ellipses. Since this angle, should be 90° , the La Toracca skew angle should be zero under 1 or 2 D conditions. In 3D conditions, the E field may be distorted (i.e. rotated), resulting in non-zero values.
m msl	meters above Mean Sea Level
Mode (TE or TM)	In a 2D world, the AMT/MT impedance is decomposed into two orthogonal components parallel (TE, or Transverse Electric) and perpendicular (TM, or Transverse Magnetic) to strike. In 1D and 3D situations the definition has limited value.
Occam inversion	Inverse modeling of geophysical data in which no <i>a priori</i> assumptions (e.g. the resistivity/thickness distribution) are made. Rather, the simplest model consistent with the data is found. Named for the 14th century philosopher William of Occam (see Occam, 1324, <i>Quodlibeta</i> , Book V: "Plurality is not to be assumed without necessity").
Period	Inverse of frequency (1/f). Commonly used instead of frequency in describing the low frequency range in AMT/MT (defined in seconds, s)
Pot	Potential electrode: sensor at the end of the E line for measuring the electric field
ρ	apparent resistivity in Ωm
ρ_{\max} and ϕ_{\max}	The higher of the two apparent resistivity curves and its associated impedance phase.
ρ_{xy}	apparent resistivity calculated from E_x and H_y
ρ_{yx}	apparent resistivity calculated from E_y and H_x

RMS error		$\sqrt{\frac{1}{npts} \sum \frac{(obs - pred)^2}{var}}$ <p>where <i>obs</i> and <i>pred</i> are the observed and predicted data responses (real and imaginary impedance tensors elements over the frequency range used and the stations employed in the inversion), <i>npts</i> is the number of data points, and <i>var</i> is the defined variance.</p>
Roughness (of resistivity model)	3D	<p>This is defined as the integral over the 3D model of $L^T L \cdot m$, where <i>L</i> is the Laplacian and <i>m</i> is the model resistivity. Interfaces in the resistivity are indicated in the model volume by zero-crossings in Roughness. In that this parameter is a fourth derivative, it is inevitably prone to noise, but in compensation aids in identifying the most likely position of an interface.</p>
Sensitivity Matrix, $A^T A$		<p>The sensitivity matrix $A^T A \equiv \frac{\Delta(response)}{\Delta(model)}$ represents the amount of change in the modeled data due to a small change in the model parameter. This shows the sensitivity of the response to a particular 3D model, for each cell of this 3D mesh.</p>
Static shift		<p>Frequency-independent shift of AMT/MT apparent resistivities along the resistivity axis, caused by local electric field distortion.</p>
Static stripping		<p>A method of correcting static shift. At a user-selected (normally high) frequency the impedance is forced to a uniform 1D solution at the actual rotation angle, such that <i>xy</i> and <i>yx</i> apparent resistivities have identical absolute values. The corresponding e-field correction is then applied for all frequencies, and impedance re-calculated at the same orientation angle. Stripping therefore attempts to correct static shift via the impedance distortion, rather than simply block-shifting the (derived) apparent resistivity curves.</p>
TD		<p>Total depth (of a well).</p>
Tipper		<p>Ratio of the vertical magnetic component H_z to the horizontal magnetic field components H_x and H_y. Since the vertical component (noise excluded) is the output of a system (the earth) to which the two horizontal components are the input, its absolute value should not exceed 1 (see <i>induction arrow</i>).</p>
Tipper strike		<p>The geographic orientation in the horizontal plane of the vector relationship between the magnetic field components (<i>tipper</i>), taking real and imaginary parts into account. In a 2D earth, the tipper strike is perpendicular to the induction arrow direction, and shows the um 2D geo-electric strike.</p>
Top of conductor		<p>A surface interpreted from a resistivity distribution (e.g. 1D layered earth models or 3D resistivity volume in the MT case) depicting the elevation of the top of the (principal) conductive horizon. Shown as contour map or line on cross-section. Units are m msl.</p>
Total conductance		<p>The conductivity (=1/resistivity), integrated to a specified depth <i>z</i>:</p> $TC = \sum_0^z \Delta z_i / \rho_i$ <p>where Δz is the thickness of the <i>i</i>th layer and ρ_i its resistivity.</p>

APPENDIX B 3D MT INVERSION MODELING

The general approach to the inversion of geophysical data consists of two steps: (1) the computation of a forward response, and (2) the comparison of this with observed data, and modification of the starting model in light of the differences between observed and computed data. To be reasonably practical, this requires a fast forward code and an efficient approach to inversion.

B.1 3D Forward Modeling

3-D MT data are derived from measurements at Earth's surface of naturally occurring electric and magnetic fields. A standard 3-D MT dataset usually comprises four complex quantities (impedances) as a function of receiver position and frequency. The four impedances observed in 3-D MT, then, are the components of a 2×2 impedance tensor. Modeling of the impedance tensor entails solving Maxwell's equations in the solid earth and atmosphere using a horizontal current source in the atmosphere to represent ionospheric and magnetospheric sources. In our modeling algorithm we divide the earth and atmosphere into rectangular blocks with the magnetic fields defined along the block edges and the electric fields defined along the normals to the block faces (Mackie et al., 1994). Finite difference equations can be easily derived using this formulation. If one eliminates the electric fields from the difference equations, one obtains a second-order set of equations in H . This system of equations is sparse, symmetric, and complex (all elements are real except for the diagonal elements). The solution to this system is obtained by use of the stabilized biconjugate gradient algorithm. Convergence is speeded up by use of a preconditioner that is the incomplete Cholesky decomposition of the diagonal sub-blocks with fill-in plus a correction for the divergence of the magnetic field (Mackie et al., 1994). Once the E and H fields have been determined for two linearly-independent source polarizations, the impedance tensor can be computed.

B.2 3D Inversion

The general magnetotelluric inverse problem is posed in canonical form and solved using the framework of Tikhonov regularization (Tikhonov and Arsenin, 1977). Following many previous workers in MT inversion, a smooth, or 'minimum-structure', resistivity model that gives acceptable fits to the observed data is sought. Thus, using a simple second-order operator, solutions are models with minimum spatial variability, or roughness. The method of nonlinear conjugate gradients (NLCG) is used to minimize the misfit; nonlinear conjugate gradients are a well-known optimization method (Fletcher and Reeves, 1959) which has been applied in a variety of nonlinear geophysical inverse problems, e.g., Ellis and Oldenburg (1994). While NLCG is a general method for optimization, it is not necessarily efficient in a computationally intensive problem like 2-D and 3-D MT inversion. The efficiency of NLCG for computing solutions of the inverse problem depends strongly on the preconditioner and the line minimization algorithm. The purpose of these is to steer the gradient into a direction in model space which parallels the final solution as much as possible. A restriction on this goal is that applying the preconditioner can require an excessive amount of computation if it is too

complicated. It is applied to a parameter vector by solving the linear system, which can therefore be applied efficiently, acting in some sense like the inverse Hessian matrix. The amount of computation needed to solve the system is less than one forward function evaluation and thus adds little overhead to the algorithm. Line minimization is only a one-dimensional problem, requiring the computation of at least one forward problem, which in 3-D MT is computationally demanding. It is thus very important to use an algorithm that does a reasonable job in the current search direction with as few trials as possible. Algorithms such as that in Press et al. (1992) do not achieve this goal. In our 3-D MT algorithm, we use a line minimization algorithm that is basically a univariate version of the Gauss-Newton method. While details of this algorithm are given in Rodi and Mackie (2001), the important result of this algorithm is that each step of the line minimization iteration requires the equivalent work of only three MT forward calculations (the real one and two pseudo ones). An additional efficiency is our choice of stopping criterion. It ensures that, when the forward problem is well-approximated by its linear approximation, each line minimization converges in a single step.

The net result is that the observed 3D data (each element of the impedance tensor, at each frequency used) can be inverted to give a smooth 3D model.

Smooth model inversions are quite useful for geologic interpretations because they provide accurate representations of the subsurface. Their disadvantage, however, is that they do not resolve sharp boundaries or interfaces. Rather, because of the smoothness constraint, interfaces are defined in general terms by resistivity gradients. Practically, however, what is of interest is the depth to a particular interface or geologic formation. In those situations where additional information is available (e.g., well logs, seismic, etc), we can use that information to generate a “tear surface” which we then project onto the MT model. Across this surface, we turn off the smoothing constraint and allow the resistivities to vary independently above and below the surface. If the geology is well approximated by this surface, then the resulting model will in general be smooth except across this surface. In this way, we can introduce sharp boundaries into the 3D MT inversion.

APPENDIX C INVERSION HISTORY

Setup	iterations	cumulative its	rms	start model	tau	tipper inversion	lnZxy amplitude	lnZxy phase	tipper error floor	reg operator	static shift	orientation [deg]	nx	ny	nz	min dx, dy [m]	min dz [m]	deep dz [m]	# sites	# frequencies	# freqs / decade	min frequency	max frequency
01_Mar26	17	17	5.307	20Ωm	0.05	y	3%	20%	0.02	Lapl	y	-16	121	99	112	800	30	100	239	21	4	0.003	300
02_Mar29	20	20	2.802	20Ωm	0.05	y	3%	20%	0.02	Lapl	y	-16	121	99	112	800	30	100	239	21	4	0.003	300
03_Mar30	3	3	-	01_20iter	0.01	y	3%	20%	0.02	Lapl	y	-16	121	99	112	800	30	100	239	21	4	0.003	300
04_Apr07	20	20	3.247	20Ωm	10	y	3%	20%	0.02	Lapl	y	-16	121	99	112	800	30	100	238	21	4	0.003	300
05_Apr08	30	50	2.525	04_20iter	3	y	3%	20%	0.02	Lapl	y	-16	121	99	112	800	30	100	238	21	4	0.003	300
06_Apr27	20	20	2.704	20Ωm	0.05	y	3%	20%	0.02	Lapl	y	-16	76	99	111	800	30	100	196	21	4	0.003	300
07_Apr30	40	60	2.115	06_20iter	0.02	y	3%	20%	0.02	Lapl	y	-16	76	99	111	800	30	100	196	21	4	0.003	300
08_Apr30	30	50	2.260	06_20iter	0.05	y	3%	20%	0.02	Lapl	y	-16	76	99	111	800	30	100	196	21	4	0.003	300

The model resulting from inversion 05 is considered the final resistivity model.

Cumulative iteration	Inversions involving a re-start (typically with lower tau, see below): total number of iteration considering also the number of previous iterations.
Rms	Root mean square: measure of data fit (see also glossary in Appendix A). Average number of standard deviation between the model data and the observed data
Tau	Regularization parameter that controls the tradeoff between fitting the data and adhering to the model constraint (larger values cause a smoother model at the expense of a worse data fit)
lnZxy amplitude (& phase), Zxx/Zyy	Error floors in % (absolute for tipper). Please not that logarithm has been calculated in the xy and yx cases
Regularization	Regularization operator measuring the model structure/roughness
Tau (m-m0)	Constraint penalizing any deviations from the a-priori model, contributing to the total objective function.
nx, ny, nz	number of cells in the x, y, z direction
min dx, min dy, min dz	minimum cell dimension in the x, y, z direction (in meters)

APPENDIX D DIGITAL DATA

All project data files are archived at Geosystem's head office in Milan, on DVD and magnetic tape.

D.1 Content

The list of digital deliverables includes:

WinGLink Database

WinGLink database, with all MT data and TDEM data and 3D inversion results.

Report

Acrobat pdf file of this report.

3D Inversion Results from Inversion Run (#5, see also Appendix C):

Plates and Resistivity Cross Sections from 3D MT inversion (Appendix E)

D.2 Output Data Formats

The output files generated by the 3D MT inversion algorithm are listed below. The name-feed

- 3dmod.out: model file, with mesh specifications and final resistivity values
- site-id_pred.edi: predicted data in EDI format
- error_d3inv.dat: containing inversion statistics,
- rmsvals.dat: listing the rms misfit for each station

D.2.1 Model File

This is an ASCII fixed-format file, which begins in the following form:

nx	ny	nz	l3	VAL					
dx1	dx2	dx3	dx,4	dx5	dx6	dx7	dx8	dx9	dx10
dx11
...	dxnx						
dy1	dy2	dy3	dy4	dy5	dy6	dy,7	dy8	dy9	dy10
dy11
...	dyny					
dz1	dz2	dz3	dz4	dz5	dz6	dz7	dz8	dz9	dz10
dz11
...	...	dznz							
1									
R1,1,1	R2,1,1	R3,1,1	R4,1,1	R5,1,1	R6,1,1
...	Rnx,1,1						
R1,2,1	R2,2,1	R3,2,1
...	Rnx,2,1						

...
R1,ny,1 R2,ny,1 R3,ny,1 R4,ny,1 R5,ny,1 R6,ny,1
... .. Rnx,ny,1
2
R1,1,2 R2,1,2 R3,1,2 R4,1,2 R5,1,2 R6,1,2
... .. Rnx,1,2
...
R1,ny,2 R2,ny,2 R3,ny,2 R4,ny,2 R5,ny,2 R6,ny,2
... .. Rnx,ny,2
3
...
...
iz
...
...
nz
R1,1,nz R2,1,nz R3,1,nz R4,1,nz R5,1,nz R6,1,nz
... .. Rnx,1,nz
...
R1,ny,2 R2,ny,2 R3,ny,2 R4,ny,2 R5,ny,2 R6,ny,2
... .. Rnx,ny,nz
WINGLINK
reference-ID (Name – arbitrary)
jx jy (jx jy – lateral indices of anchor-cell)
easting northing (real world coordinates of anchor, center of above cell, in km)
angle (Orientation of mesh, angle for X-axis, in degrees N from E)
elevation (Elevation of the model top, in km)

In this, the first three numbers indicate the number of cells in the x, y, and z directions, respectively, and the following rows list the cell dimensions in meters. Upon these dimension sections, resistivity values are listed layer by layer, with the vertical index preceding each layer section.

The model anchor, necessary to locate the 3D model in real coordinates, is given at the bottom of the file. After an arbitrary ID string, the two lateral indices jx and jy mark the cell used for the anchoring (usually 1, 1). The two real numbers in the following line give the coordinates in km in the (e.g. UTM – see section 1) of the *center* of that cell.

Note this convention is different to the anchor definition within the WinGLink software, where the anchor is the NW corner of the reference cell. The WinGLink import routine automatically re-calculates the anchor position, and therefore these values – as well as all other values except for the model name – do not need to be entered when importing.

The coordinate system of the model is x: positive East, y: positive South, and z: positive Down. Therefore the rotation angle (given in the next line) is defined as positive North from East. As the MT data angle by standard convention is positive East from North, the data need to be rotated for the modeling such that both angles add up to 90 degrees.

The last line gives the elevation in km of the model top.

D.2.2 Predicted Data

The computed responses are output in separate EDI files (Wight, 1988), one per site. These contain the frequencies and computed impedances corresponding to the final 3D inversion models, in the same coordinate system and rotation angle as the input data files.

D.2.3 Inversion Log and Data Misfit

The inversion log lists the inversion parameters, and the overall RMS misfit and objective function values at each iteration. The separate file on RMS lists the misfit between the observed and computed responses at each station, for the last iteration.

APPENDIX E RESISTIVITY PLATES AND CROSS SECTIONS

The resistivity color scale is identical for all resistivity maps and cross-sections.

E.1 Maps

MT station and profile locations are shown on topographic base map in Plate 1. The 3D resistivity mesh is illustrated via depth slice maps in Plates 2a-l, from -250m to -5000m msl. Scale 1:350,000.

E.2 Cross Sections

Resistivity cross-sections (Ωm) from smooth 3D inversions are plotted for main profiles A, B, C, and B1, D, D1, and six additional profiles (B1, D, D1, EW-1, EW-11, EW-2) between these. Horizontal and vertical scales are at 1:150,000 and 1:75,000, respectively. Vertical exaggeration is 2.